Power-dependent effective reflection of fiber Bragg grating as output coupler of Ytterbium-doped fiber laser

Yuri O. Barmenkov [a],[1], Pablo Muniz-Cánovas [a],[2], Alexander V. Kir'yanov [a],[3], Vicente Aboites [a],[4],[*], José-Luis Cruz [b],[5], Miguel V. Andrés [b],[6]

[a] Centro de Investigaciones en Óptica, A.C., Loma del Bosque 115, 37150 Leon, Gto., Mexico
[b] Departamento de Física Aplicada, Instituto de Ciencia de Materiales, Universidad de Valencia, 46100 Valencia, Spain

ARTICLE INFO

ABSTRACT

In this paper, we discuss the effective reflection of a fiber Bragg grating and its dependence on laser power when it is used as an output coupler of an ytterbium-doped fiber laser (here the effective reflection is considered to be a part of intracavity laser power reflected by the grating back to the laser cavity). We propose and discuss an experimental technique based on spectral and power analysis and derive simple formulae that permits one to obtain the intra-cavity power and the grating effective reflection. We show that, due to spectral broadening, the effective reflection dramatically decreases with increasing laser power, the effect precisely fitted using the derived formulae describing this quantity. The experimental part of the present study is based on an analysis of the operational regime of a long-wavelength ytterbium-doped fiber laser.

Introduction

Fiber lasers are versatile light sources that can operate in continues-wave (CW) [1], Q-switching [2,3], mode-locking [4] including noise [5] and soliton [6] pulsing, single-frequency [7], noise CW [8] and other regimes. CW Ytterbium-doped fiber lasers (YDFLs) are highly efficient oscillators with optical efficiency as high as ~80% [9–11], limited mostly by the Stokes-shift loss. Usually YDFLs operate within the "conventional" Yb^{3+} emission band, ~1040 nm to 1120 nm with output power reaching multi-kW [9–13] and even hundred-kW [13–15] levels. Due to the ideal power budget and very large power scaling, these FLs found a number of technical applications.

YDFLs are also capable to operate in the long-wavelength (LW) range, viz. from 1120 nm to 1200 nm [16–18]. YDFLs of this class are of special practical interest because of combination of their excellent energetic properties and the operational spectral band in which diode lasers cannot compete due to the technological problems. Specifically, LW-YDFLs are applicable as pump sources for a line of FLs (such as

Ho-doped and Raman (random) FLs [19–23]) and for frequency-doubling ("yellow light" [24,25]). Besides, laser sources operating in this range found other important applications, say, in the minimally invasive harmonic generation microscopy [26], medical diagnostics [27] etc.

However, a disadvantage inherent to LW-YDFLs is that laser signal in this case competes with a strong amplified spontaneous emission (ASE) arising within the "conventional" spectral band, ~1060 to 1100 nm [16,28], due to a very high gain in YDF in this spectral range as compared that inherent to LWs. Moreover, the higher pump power, the stronger ASE signal is; so with increasing pump power above some critical level, CW parasitic lasing (PL) arises at some wavelength within this spectral band [28,29] when a high YDF gain gets compensating a high-level loss of the parasitic cavity formed by weak reflections from the laser-cavity components and fiber splices. With pump power growth, the efficiency of lasing at a LW drops due to both the increase of ASE spectral density and PL power. Meanwhile, parasitic PL may, in turn, produce high-power pulsing ignited by stimulated Brillouin scattering

* Corresponding author.
[1] ORCID: 0000-0002-0963-833X.
[2] ORCID: 0000-0002-0300-2701.
[3] ORCID: 0000-0002-4794-6763.
[4] ORCID: 0000-0003-0276-6774.
[5] ORCID: 0000-0002-4360-9989.
[6] ORCID: 0000-0003-0103-8644.

(SBS) [29,30], the phenomenon that usually stands behind the damage of YDF used as an active fiber [29,31]. Also note that SBS pulsing in YDFLs operating in the 'conventional' wavelength range is inherent in laser cavities with a low Q-factor [30].

To clarify the physics behind PL in LW-YDFLs, we studied the processes relevant to the pump-dependent variation in 'effective' reflectivity of the laser output coupler (a weakly reflective fiber Bragg grating, FBG). This variation leads to a change of 'effective' Q-factor of the cavity and, hence, to a change in the active fiber gain, too. We show that the effective (factual) reflection of the FBG dramatically depends on the laser power, the effect related to strong broadening of CW YDFL spectrum [32,33] through the nonlinear effects in optical fiber, namely, by self-phase modulation (SPM) originated from Kerr effect and initiated by a fluctuating laser power [32,34,35]. Furthermore, we present a simple experimental technique permitting one to measure the effective FBG reflection as a function of YDFL laser power and its mathematical assessment including simple analytic formulae that describe variations in the FBG effective reflection. We believe that our present work is important for understanding the physics involved in CW FLs operating, including in the LW range, at moderate powers (watts to tens watts) and, also, for their modeling and optimization.

Note that the use of FBGs as selective reflectors permits one to assemble FL cavity in a robust all-fiber geometry; they also may modify the laser operation mode after a correspondent fiber treatment related, for instance, to the novel materials based on the nonlinear electromagnetically induced transparency [36,37]. Also note that the term "effective" length of a FBG placed inside a short Fabry-Pérot laser cavity, introduced in our earlier works [38,39], defines the factual length of the laser cavity and, consequently, the real optical frequencies of longitudinal modes established in it.

Laser setup and basic characteristics

Our YDFL was assembled in Fabry-Pérot geometry, common for high-power FLs. Fig. 1(a) presents the experimental setup. A standard double-clad YDF (Nufern, SM-YDF-5/130-VIII) was used as an active (gain) medium. YDF was relatively long: its length was 30 m that produces a high absorption (~20 dB) at the pump wavelength ($\lambda_p = 915$ nm) and ensures ease of lasing in the LW Yb^{3+} emission band. Note that YDF was pumped by two 30-W laser diodes (LDs) with multimode fiber outputs through a commercial $(2 + 1) \times 1$ pump combiner with the waveguide parameters of its signal and pump fibers similar to those of both the YDF and LDs' output fibers.

Two home-made FBGs with the reflection coefficients of ~100% (high-reflection (HR)-FBG) and ~38% (low-reflection (LR)-FBG) where used as the rear and output cavity couplers, respectively; the peak reflection of the LR-FBG is herewith designated as R_0. The FBGs' reflection spectra are demonstrated in Fig. 1(b). It is seen from this figure that reflection maxima of both FBGs were at $\lambda_s = 1134.7$ nm (the

laser wavelength that belong to the LW Yb3 + emission band), and that the FBGs' bandwidths measured at FWHM (full width as half of maximum) were correspondingly 480 pm (HR-FBG) and 220 pm (LR-FBG). Resolution of the optical spectrum analyzer (OSA, Yokogawa, model AQ6370D, wavelength range from 600 nm to 1700 nm) used in this experiment was 31 pm at the laser wavelength.

The reflection band of the HR-FBG has been managed to be as broad as possible (to maintain approximately 100%-reflection in the whole range of the laser power from 0 to 30 W) with an aim to minimize the decreasing of the laser power transmitted by any HR-FBG due to "spectral surrounding" of its reflection spectrum, the effect eventually resulted from spectral broadening of a laser signal at a high laser power [32–34]. The reflectivity of the LR-FBG was high enough to ensure maintaining of the tuning range of pump power as high as 60 W without arising PL within the "conventional" Yb^{3+} band (see above). For the same reason, the YDF was heated up to 40 °C [16,28]. Furthermore, to diminish the thermal shift of the gratings' Bragg wavelengths, they were mounted on aluminum heat dissipaters; this allowed us to minimize the spectral shift of the laser peak wavelength lesser than 1 pm per 1 Watt of laser power.

A cladding mode stripper (CMS) was used to remove the residual pump at the input of the LR-FBG written in a single-mode fiber. To decrease the Fresnel reflections we used 7°-angled fiber cuts on both sides of the laser.

The laser power was measured by a commercial power meter (Thorlabs, model PM100D) with a thermal head (Thorlabs, model S322C, maximum power is 200 W). From Fig. 2(a), it is seen that the output laser power depends linearly on the pump power; the laser threshold was 0.6 W, the power slope efficiency was 53% and the quantum slope efficiency was 66%. Note that such moderate laser efficiencies are common for LW-YDFLs [27–29] because of the large Stokes shift (~25% relatively to the pump wavelength) and strong ASE arising within the "conventional" Yb^{3+} emission band.

Fig. 2(b) shows the broadband YDFL spectrum measured at four pump powers. It is seen that ASE spectrum is always within the range ~1060 nm to ~1120 nm; its peak value pronounceably grows with increasing pump power, with the rate of 0.45 dB/W, while the laser spectral peak grows with the smaller rate, of 0.29 dB/W or less. Simultaneously, ASE spectral peak shifts to the anti-Stokes side, from 1090 nm to 1070 nm, where YDF gain is higher. Worth noticing, the CW PL at ~1060…1080 nm, potentially dangerous as igniting SBS pulsing (see above), arises in our experimental conditions at the highest pump power (around 60 W).

Narrowband laser spectra

Fig. 3(a) shows the YDFL spectra measured in the whole range of laser power. As it is seen, the laser spectrum dramatically broadens with increasing laser power, the effect related to the nonlinear phenomena in
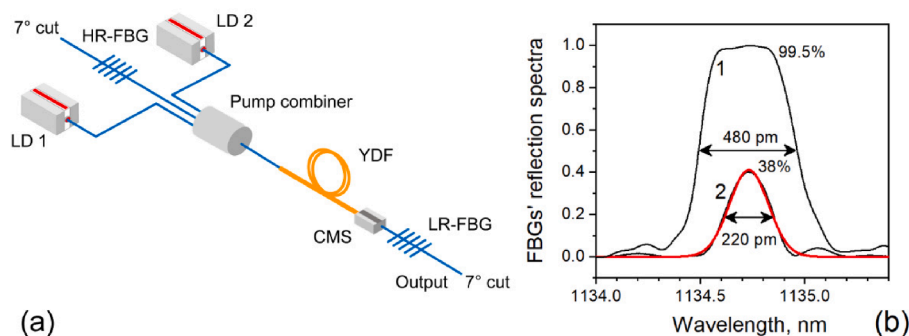

Fig. 1. (a) YDFL setup. LD1 and LD2 are laser diodes, CMS is cladding mode stripper. (b) Reflection spectra of the rear (curve 1) and the output (curve 2) FBGs. Red line shows the Gaussian fit of the LR-FBG spectrum. (For interpretation of the references to colour in this figure legend, the reader is referred to the web version of this article.)
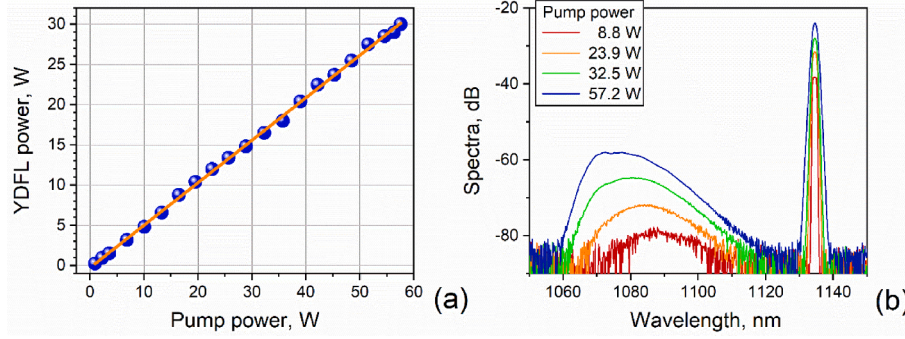
Fig. 2. (a) YDFL power *vs* pump power. The blue circles stand for the experimental points and the orange line – for the linear fit. (b) Broadband YDFL spectra measured at four pump powers (see inset). The OSA resolution is 1 nm. (For interpretation of the references to colour in this figure legend, the reader is referred to the web version of this article.)
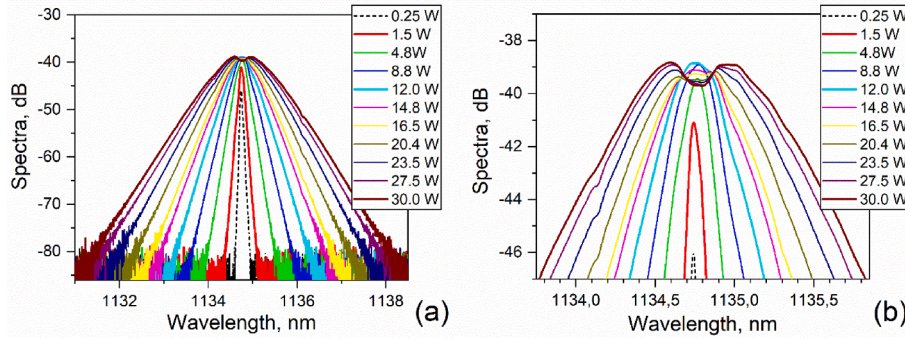

Fig. 3. (a) Narrowband YDFL spectra measured with the OSA resolution of 31 pm. (b) The same spectra presented at zooming the wavelength range. The laser powers at which the spectra were measured are indicated in the insets.

optical fibers (mostly due to SPM), arisen at such power values at which the Kerr-effect produces nonlinear phase exceeding ~1 rad. [35]; this condition is satisfied in the YDFL under study when CW laser power exceeds 10 W. Furthermore, since the narrow-band CW YDFLs demonstrate excessive photon noise with the photon statistics described by the Bose-Einstein distribution [8] – when noise peaks reach power levels above the mean (CW) laser power by an order of value or more – the laser spectrum gets broadened yet at lower laser powers, of ~1 W. Note here that the laser spectra, measured at low laser powers (below 10–15 W) and plotted in the logarithmic (dB) scale, are characterized by symmetrical triangular shape, which corroborates with the noise behavior of the laser signal. That is, the derivative of the instantaneous laser power, responsible for the laser spectrum broadening, demonstrates similar (triangular) shaping of the probability density function likewise that of the laser spectrum, refer to Fig. 3.11 in ref. [40]. At further growth of the laser power, a notable dip arises at the spectrum center, which is due to overlapping of the transmission spectrum of the LR-FBG with the broadened laser spectrum: see Fig. 3(b). Note that such kind of the spectral hole burning effect was recently reported in [41].

Effective reflection of the output FBG: theory

Given that the YDFL spectrum strongly broadens with laser power growth, a part of the laser signal with spectral components outside the LR-FBG spectrum, dramatically increases. This part is not reflected by the grating at all or is reflected with smaller efficiency. This effect can be treated in terms of the power-dependent effective reflection of the grating, which decreases with the laser power increase. The latter results in diminishing the Q-factor of the laser cavity and enlarging the YDF gain that compensates the cavity loss growth.

We consider the effective reflection of the output (LR) FBG as a ratio of laser power reflected by the grating to the incidence power:

$$R_{eff} = \frac{P_{refl}}{P_{cav}} = \frac{P_{cav} - P_{out}}{P_{cav}} \tag{1}$$

where P_{refl} is the optical power reflected by the FBG, P_{out} is the laser output power, and P_{cav} is the intracavity laser power at the FBG input. Thus, to calculate R_{eff} one needs to know the output laser power, P_{out}, spectrum of the output laser signal, $S_{out}(\lambda)$, and the FBG reflection spectrum, $R_{FBG}(\lambda)$. These data are easily obtained from the power and spectral measurements, see Fig. 2(a), 3 and 4. To simplify the simulation of the intracavity laser spectra, a Gaussian fit, obtained with high precision (adjusted R-square is 0.993), was used as the FBG reflection spectra (see Fig. 1(b)).

The intracavity laser spectrum at the FBG input (further, the intracavity laser spectrum) is found as follows:

$$S_{cav}(\lambda) = \frac{S_{out}(\lambda)}{T_{FBG}(\lambda)} = \frac{S_{out}(\lambda)}{1 - R_{FBG}(\lambda)} \tag{2}$$

where $T_{FBG}(\lambda) = 1 - R_{FBG}(\lambda)$ is the FBG transmission spectrum. The intracavity laser power at the same point of the laser cavity is obtained as:

$$P_{cav} = \xi \int_{\lambda_1}^{\lambda_2} S_{cav}(\lambda) d\lambda \tag{3}$$

where the proportionality coefficient, ξ, is found from the following formula:

$$\xi = \frac{P_{out}}{\int_{\lambda_1}^{\lambda_2} S_{out}(\lambda) d\lambda} \tag{4}$$

In these two equations, the interval from λ_1 to λ_2 is that within which the FBG and the laser spectra are not equal to zero.

Fig. 4 shows two examples of simulating of $S_{cav}(\lambda)$ using $S_{out}(\lambda)$ along with the FBG reflection and transmission spectra. At very low laser powers (e.g. at 0.25 W, Fig. 4(a)), the laser output and the intracavity spectra are similar; their magnitudes differ by approximately 60% that equals to the peak FBG transmission. This result is explained by the fact that the laser spectrum is quite narrow as compared to that of the FBG (their widths measured at FWHM are 45 pm and 220 pm, respectively) whilst the variation in the FBG reflection near its peak is small. At high laser powers (e.g. at 30 W, Fig. 4(b)), the shapes of the spectra differ much stronger: the broadened laser output spectrum has two peaks that arise due to reflection from the spectrally narrow LR-FBG (compare with the spectra in Fig. 3(b) for laser power above 20 W). In the meantime, the intracavity laser spectrum demonstrates a single peak while its sections outside the FBG spectrum are identical to the output laser spectrum.

Fig. 5 shows the intracavity laser spectra for the whole range of laser powers, calculated using the formulae presented above. As it is seen from Fig. 5(a), these spectra do not demonstrate a double-peak structure at high laser power: compare them with the spectra shown in Fig. 3. Then, as seen from Fig. 5(b) (where the same spectra but zoomed are shown), the maximum density of the laser spectral peak is observed in the range of laser powers between 8 and 13 W. This effect results from the strong spectral broadening that arises in the YDFL when the laser power exceeds 10 W and so the nonlinear phase increases up to the values well above 1 rad. [35]. We found, using the theory presented in [35], that the laser power at which the nonlinear phase is equal to 1 rad. is about 8 W; this value is close to that at which the spectral density at the laser peak wavelength takes a maximum. Note that the spectral broadening is so strong that the spectral density at the top decreases despite the integral spectral power increases. This detail is virtually undetectable when one examines the original laser spectra (Fig. 3).

Using the procedure described above, which is based on (*i*) the spectral analysis of the laser output signal (Fig. 3) along with the LR-FBG spectrum (Fig. 1(b)) and (*ii*) the data on the laser output power (Fig. 2 (a)), we can obtain the intracavity laser power, P_{cav} (see formulas (2)–(4)), and the effective reflection, R_{eff}, of the grating (see formula (1)). Since all the data used in the calculus are experimental, we consider the resultant data for R_{eff} (see Fig. 7 below) as experimental, too.

Effective reflection of the output FBG: simulation

First, we found, using Eqs. (2)–(4), the intracavity power P_{cav} at the LR-FBG input for the whole range of laser (output) power; the result is shown in Fig. 6. It is seen that P_{cav} is always above P_{out}, the difference between them is the power reflected by the LR-FBG: $\Delta P = P_{cav} - P_{out}$ (see Fig. 6(a)). At low P_{out}, this difference increases exponentially (Fig. 6(b)) until it gets saturated at some ΔP_0 value (2.75 W in our case). Thus, the

LR-FBG reflects approximately the same power ($P_{refl} = \Delta P_0 = 2.75$ W) for any laser power exceeding approximately 15 W. This effect results in that the blue line fitting data for the intra-cavity power above 15 W becomes parallel to the black one corresponding to the laser output power, see Fig. 6(a).

For comparison, we also show the dependence of the laser spectrum width, measured as FWHM, with the laser output power increase, see Fig. 6(b). It is seen that the spectrum width increases faster at high laser power, above 15 W, than it takes place at lower power; the difference in the slope of this dependence above and below 15 W is about two times. This effect is related to the rise, with increasing pump power, of the nonlinear phase shift up to the value above which the laser spectral line gets broaden faster, see the discussion in the previous section.

Let us consider that P_{refl} increases with laser output power by the saturating exponential law:

$$P_{refl} = \Delta P_0 \left[1 - \exp\left(-\frac{P_{out}}{P_0} \right) \right] \tag{5}$$

where $P_0 = 4.39$ W is the power at which P_{refl} differs by $(1 - e^{-1})$ times from the maximum value. Despite this law is empirical, it fits the experimental points shown in Fig. 6(b) by curve 1 with a very high accuracy: R-square is higher than 0.999. Using Eq. (5) one can rewrite Eq. (1) as follows:

$$R_{eff} = \frac{\Delta P_0 \left[1 - \exp\left(-\frac{P_{out}}{P_0} \right) \right]}{P_{out} + \Delta P_0 \left[1 - \exp\left(-\frac{P_{out}}{P_0} \right) \right]} \tag{6}$$

Using this equation, we fitted the set of R_{eff} points found from Eqs. (1)-(4) with a high accuracy, too (*R*-square is higher than 0.996); see Fig. 7. At very low laser power, $R_{eff} = \Delta P_0/(P_0 + \Delta P_0) \approx R_0$, given that the laser spectrum is narrow due to the absence of nonlinear effects and that it matches the LR-FBG peak wavelength (refer to Fig. 4(a)). At higher laser power, R_{eff} decreases with increasing P_{out} as the hyperbolic function: $R_{eff} \approx \Delta P_0/P_{out}$.

Furthermore, one can see from Fig. 7 that R_{eff} steadily decays by approximately-one order of magnitude, from ~40% to ~8%, with laser power growth. The experimental R_{eff} points are fitted well by formula (6) when $P_0 = 4.54$ W. This value is very close to that found from the fitting of the power reflected by the LR-FBG ($P_0 = 4.39$ W). Note that both the parameters determining the grating's effective reflection P_0 and ΔP_0, depend on its reflection spectrum width, too: the narrower the reflection peak, the smaller is the reflected power, and *vice versa*. Thus, a proper choice of the reflection band of a LR-FBG is advisable for estimating its effective (factual) reflection and, consequently, for realistic understanding of how the active fiber gain in a FL depends upon laser power.

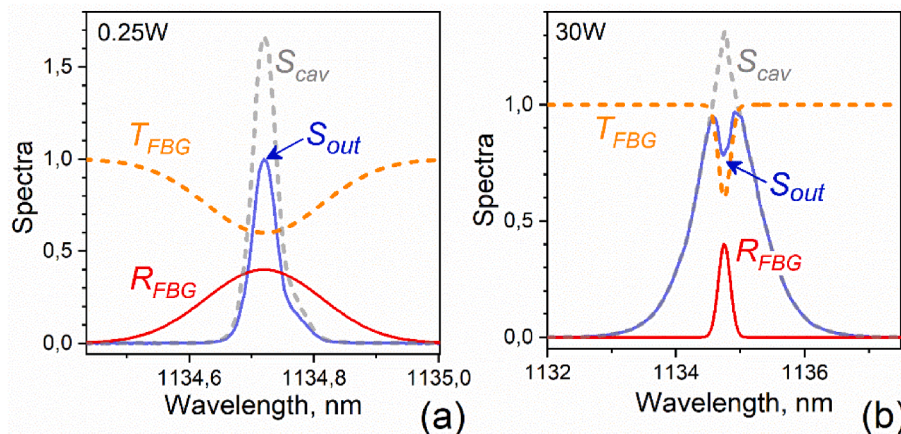A remark: in the above modeling, we ignored a small thermal shift to

Fig. 4. Normalized experimental laser output spectra S_{out} (the blue solid lines), simulated laser intra-cavity spectra at the FBG input S_{cav} (the grey dash lines), and FBG reflection (the red solid lines) and transmission (the orange dash line) spectra. S_{cav} and S_{out} are normalized to the peak value of S_{out}. The laser output power is (a) 0.25 W and (b) 30 W. Note that the scaling factor of the horizontal (wavelength) axes in (a) and (b) differs by an order of value and the vertical axes are linear. (For interpretation of the references to colour in this figure legend, the reader is referred to the web version of this article.)
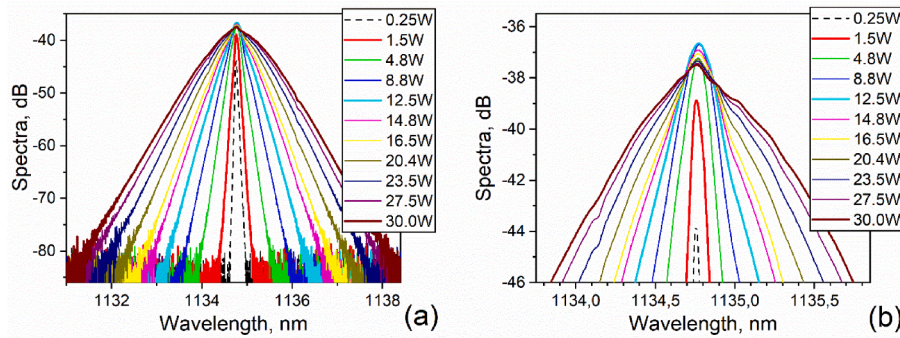
Fig. 5. (a) Simulated YDFL intracavity spectra presented in the whole wavelength range and (b) in the zoomed range, revealing the spectral behavior in more detail. The laser powers are indicated in the insets.
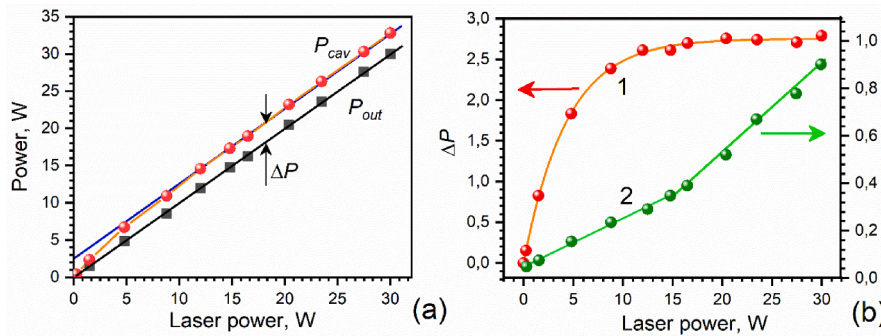

Fig. 6. (a) The intracavity power (P_{cav}, the orange circles and curve) *vs* laser output power; the laser output power (P_{out}, the black squares and line) is shown for comparison; ΔP is the difference between these two graphs. The symbols stand for the experimental data and the lines are their fits. The blue line shows a linear fit of the intracavity power at $P_{out} > 12$ W. (b) Curve 1: ΔP *vs* laser output power (the left scale); the points stand for the experimental data and the curve is their exponential fit. Curve 2: Spectrum width of the intracavity laser signal *vs* laser power (the right scale); the points are data obtained for the spectra shown in Fig. 5 and the lines are linear fits for low (below 15 W) and high (above 15 W) laser power. (For interpretation of the references to colour in this figure legend, the reader is referred to the web version of this article.)
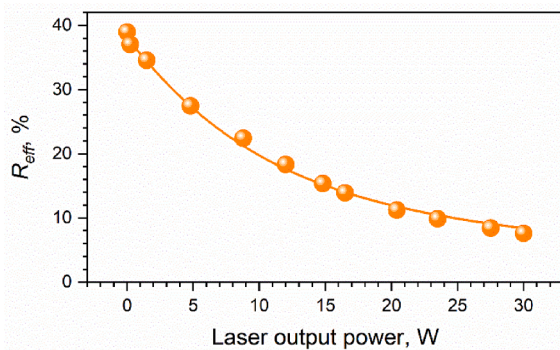

Fig. 7. Effective reflection of LR-FBG (R_{eff}) *vs* laser output power. The circles and the solid line show, correspondingly, the experimental data and their fit obtained using formula (6).

the Stokes side of the LR-FBG Bragg wavelength with increasing laser power since it is much less than the 3 dB-bandwidth of the HR-FBG used as the rear reflector of the cavity, see our discussion in Section "Laser setup and basic characteristics".

Conclusions

In this paper, we introduced the effective reflection (R_{eff}) of an output (low-reflecting, LR) FBG coupler of an YDFL as a ratio of the optical power returned by the FBG to the laser cavity to the optical power at the FBG incidence. A CW YDFL based on a standard Ytterbium-doped double-clad fiber with 5-μm core operated at a long wavelength (~1.135 μm) was chosen for the current study. To find R_{eff} we proposed a simple experimental technique permitting an analysis of output laser spectra, FBG spectrum, and laser power; we also derived simple formulae for simulating R_{eff}.

We showed that the power reflected by the LR-FBG coupler back to the laser cavity increases by the exponential law at relatively low (<10 W) laser powers. Meanwhile, at laser power exceeding 10 W, the LR-FBG reflects the same power independently of laser power. The latter is resulted from the strong broadening of the laser line due to the nonlinear (Kerr) effect so that the spectral density at the laser spectrum peak (at the LR-FBG incidence) and in the narrow area in its proximity virtually does not change despite the integral spectral power increases linearly with increasing the laser output power.

It was found that the effective reflection of the output LR-FBG decreases with increasing laser power, which happens because of broadening of the laser spectrum and so results in passing by a considerable part of laser power off the LR-FBG reflection spectrum. At a high laser power, the effective decrease in LR-FBG's reflection is close to the hyperbolic law: $R_{eff} \sim (P_{out})^{-1}$.

The revealed effect results in increasing the laser cavity loss and, therefore, enlarging the active fiber gain needed for its compensation to maintain the CW laser regime. The latter feature may result, in the case of an YDFL operating at a long wavelength, in the appearance of parasitic lasing within the "conventional" Yb^{3+} emission band (1060…1100 nm), deteriorating the laser regime.

We believe that the clue element of the present study, viz. the role of the effective (power-dependent) reflection of a FBG output coupler, can be important for understanding the detailed physics of YDFLs operating at moderate laser powers (Watts to tenths of Watts) at longer operational wavelengths and their proper modeling.

Declaration of Competing Interest

The authors declare that they have no known competing financial interests or personal relationships that could have appeared to influence the work reported in this paper.

Data availability

Data will be made available on request.

References

[1] Hu Q, Zhao X, Tian X, Wang M, Wang Z, Xu X. Raman suppression in high-power fiber laser oscillator by long period fiber grating. Res Phys 2021;26:104460. https://doi.org/10.1016/j.rinp.2021.104460.

[2] Escalante-Zarate L, Barmenkov YO, Kolpakov A, Cruz JL, Andrés MV. Smart Q-switching for single-pulse generation in an erbium-doped fiber laser. Opt Express 2012;20(4):4397–402. https://doi.org/10.1364/OE.20.004397.

[3] Radzi NM, Latif AA, Ismail MF, Liew JYC, Wang E, Lee HK, et al. Q-switched fiber laser based on CdS quantum dots as a saturable absorber. Res Phys 2020;16: 103123. https://doi.org/10.1016/j.rinp.2020.103123.

[4] Zhou X, Yang Q, Wang Z, Zhang Z. Mode-locked thulium-doped fiber laser with microfiber based polarization beam splitter. Res Phys 2020;18:103261. https://doi.org/10.1016/j.rinp.2020.103261.

[5] Gonzalez-Galicia MA, Lozano-Crisostomo N, Barmenkov Y. Time-bandwidth product of noise-like pulses within the mode-locked regions of a figure-eight fiber laser: theoretical and experimental analysis. J Opt Soc Am B 2021;38(10):3150–8. https://doi.org/10.1364/JOSAB.437522.

[6] Ahmed MHM, Yusoff NM, Abdullah CAC, Alresheedi MT, Rosli NS, Talib ZA, et al. Nanosized titanium dioxide saturable absorber for soliton mode-locked thulium-doped fiber laser. Res Phys 2021;31:104930. https://doi.org/10.1016/j.rinp.2021.104930.

[7] Barmenkov YO, Kir'yanov AV, Pérez-Millán P, Cruz JL, Andrés MV. Experimental study of a symmetrically-pumped distributed feed-back Erbium-doped fiber laser with a tunable phase shift. Laser Phys Lett 2008;5(5):357–60.

[8] Muniz-Cánovas P, Barmenkov YO, Kir'yanov AV, Cruz JL, Andrés MV. Ytterbium-doped fiber laser as pulsed source of narrowband amplified spontaneous emission. Sci Rep 2019;9(1). https://doi.org/10.1038/s41598-019-49695-9.

[9] Richardson DJ, Nilsson J, Clarkson WA. High power fiber lasers: current status and future perspectives [Invited]. J Opt Soc Am B 2010;27(11):B63–92. https://doi.org/10.1364/JOSAB.27.000B63.

[10] Jeong Y, Sahu JK, Payne DN, Nilsson J. Ytterbium-doped large-core fiber laser with 1.36 kW continuous-wave output power. Opt Express 2004;12(25):6088–92. https://doi.org/10.1364/OPEX.12.006088.

[11] Zheng J, Zhao W, Zhao B, Hou C, Li Z, Li G, et al. 4.62 kW excellent beam quality laser output with a low-loss Yb/Ce co-doped fiber fabricated by chelate gas phase deposition technique. Opt Mater Express 2017;7(4):1259–66. https://doi.org/10.1364/OME.7.001259.

[12] Wang Y, Gao C, Tang X, Zhan H, Peng K, Ni Li, et al. 30/900 Yb-doped Aluminophosphosilicate fiber presenting 6.85-kW laser output pumped with commercial 976-nm laser diodes". J Lightw Technol 2018;36(16):3396–402.

[13] Zervas MN, Codemard CA. High power fiber lasers: A review. IEEE J Sel Topics Quant Electron 2014;20(5):0904123. https://doi.org/10.1109/JSTQE.2014.2321279.

[14] Ferin A, Gapontsev V, Fomin V, Abramov A, Abramov M, Mochalov D. 31.5 kW CW fiber laser with 100 μm delivery, presented at 15th Int Conf Laser Opt, St. Petersburg, Russia 2012; paper TuSY1-1.4. https://doi.org/10.1364/ASSL.2013.ATh4A.2.

[15] Shcherbakov EA, Fomin VV, Abramov AA, Ferin AA, Mochalov DV, Gapontsev VP. Industrial grade 100 kW power CW fiber laser, in Proc Adv Solid-State Lasers Congr Tech Dig, San Diego, CA, USA 2013; paper ATh4A.2. https://doi.org/10.1364/ASSL.2013.ATh4A.2.

[16] Jacquemet M, Mugnier A, Le Corre G, Goyat G, Pureur D. CW PM multiwatts Yb-doped fiber laser directly emitting at long wavelength. IEEE J Select Topics Quant Electron 2009;15(1):120–218. https://doi.org/10.1109/JSTQE.2008.2010832.

[17] Zhou P, Wang X, Xiao H, Ma Y, Chen J. Review on recent progress on Yb-doped fiber laser in a variety of oscillation spectral ranges. Las Phys 2012;22(5):823–31. https://doi.org/10.1134/S1054660X12050404.

[18] Zhou P, Li R, Xiao H, Huang L, Zhang H, Leng J, et al. Exploring high power, extreme wavelength operating potential of rare-earth-doped silica fiber. Proc SPIE 2017;10339:103391C. https://doi.org/10.1117/12.2269614.

[19] Hemming A, Simakov N, Haub J, Carter A. A review of recent progress in holmium-doped silica fibre sources. Opt Fiber Technol 2014;20(6):621–30. https://doi.org/10.1016/j.yofte.2014.08.010.

[20] Kir'yanov AV, Barmenkov YO, Villegas-Garcia IL, Cruz JL, Andres MV. Highly efficient holmium-doped all-fiber ~2.07-μm laser pumped by ytterbium-doped fiber Laser at ~1.13 μm. IEEE J Select Topics Quant Electron 2018;24(5):1–8.

[21] Kopyeva MS, Filatova SA, Kamynin VA, Trikshev AI, Kozlikina EI, Astashov VV, et al. Ex vivo exposure to soft biological tissues by the 2-μM all-fiber ultrafast holmium laser system. Appl Sci 2022;12(8):3825. https://doi.org/10.3390/app12083825.

[22] Du X, Zhang H, Wang X, Zhou P, Liu Z. Short cavity-length random fiber laser with record power and ultrahigh efficiency. Opt Lett 2016;41(3):571–654. https://doi.org/10.1364/OL.41.000571.

[23] Chen Y, Fan C, Yao T, Xiao H, Leng J, Zhou P, et al., Brightness enhancement in random Raman fiber laser based on a graded-index fiber with high-power multimode pumping, Opt Lett 2021; 46(5):1185-1188. https://doi.org/10.1364/OL.416740.

[24] Sinha S, Langrock C, Digonnet MJF, Fejer MM, Byer RL. Efficient yellow-light generation by frequency doubling a narrow-linewidth 1150 nm ytterbium fiber oscillator. Opt Lett 2006;31(3):347–439. https://doi.org/10.1364/OL.31.000347.

[25] Bacher C, Oliveira R, Nogueira RN, Romano V, Ryser M. Yellow light generation by frequency doubling of a fiber oscillator. Proc SPIE 2016;9893:989303. https://doi.org/10.1117/12.2230681.

[26] Huang J, Guo L, Wang J, Li T, Lee H, Chiu P, et al. Fiber-based 1150-nm femtosecond laser source for the minimally invasive harmonic generation microscopy. J Biomed Opt 2017;22(3):036008. https://doi.org/10.1117/1.JBO.22.3.036008.

[27] Liu T, Huang J, Guo L, Wang J, Li T, Lee H, Chiu P, Peng L. Fiber-based 1150-nm femtosecond laser source for the label-free virtual optical biopsy (Conference presentation). Proc. SPIE 2018, Optical Fibers and Sensors for Medical Diagnostics and Treatment Applications XVIII; 10488:1048803. https://doi.org/10.1117/12.2286768.

[28] Dvoyrin VV, Medvedkov OI, Sorokina IT. YDFL operating in 1150–1200-nm spectral domain. IEEE J Quant Electron 2013;49(4):419–25. https://doi.org/10.1109/JQE.2013.2250255.

[29] Xiao H, Zhang H, Xu J, Leng J, Zhou P. 120 W monolithic Yb-doped fiber oscillator at 1150 nm. J Opt Soc Am B 2017;34(3):A63–9. https://doi.org/10.1364/JOSAB.34.000A63.

[30] Barmenkov YO, Muniz-Canovas P, Kir'yanov AV, Carrascosa AA, Cruz JL, Andres MV. Coexistence of quasi-CW and SBS-boosted self-Q-switched pulsing in Ytterbium-doped fiber laser with low Q-factor cavity. J Lightw Technol 2020;38 (14):3751–8.

[31] Ye C, Yan P, Huang L, Liu Q, Gong M. Stimulated Brillouin scattering phenomena in a nanosecond linearly polarized Yb-doped double-clad fiber amplifier. Laser Phys 2007;4(5):376–81. https://doi.org/10.1002/lapl.200610123.

[32] Kablukov SI, Zlobina EA, Podivilov EV, Babin SA. Output spectrum of Yb-doped fiber lasers. Opt Lett 2012;37(13):2508–10. https://doi.org/10.1364/OL.37.002508.

[33] Ying H, Yu Y, Cao J, Huang Z, Pan Z, Wang Z, et al. 2 kW pump-light-stripper-free distributed side-coupled cladding-pumped fiber oscillator. Las Phys Lett 2017;14 (6):065102. https://doi.org/10.1088/1612-202X/aa6dc8.

[34] Bednyakova AE, Gorbunov OA, Politko MO, Kablukov SI, Smirnov SV, Churkin DV, et al. Generation dynamics of the narrowband Yb-doped fiber laser. Opt Express 2013;21(7):8177–82. https://doi.org/10.1364/OE.21.008177.

[35] Agrawal GP. Nonlinear Fiber Optics, 3rd ed. Chapter 4. Academic Press. ISBN: 978-0-080-47974-3.

[36] Varmazyari V, Parvin P, Eilchi M, Mousavi NS, Habibiyan H, Ghafoorifard H. An adjustable EIT-based FBG in Yb:silica master-oscillator fiber power-amplifier system. IEEE J Quant Electron 2018;54(4):6800409. https://doi.org/10.1109/JQE.2018.2847420.

[37] Mousavi NS, Parvin P, Ilchi-Ghazaani M. Fiber Bragg grating-electromagnetically induced transparent fast optical switch. OSA Continuum 2021; 4:1473-1487. https://doi.org/10.1364/OSAC.415468.

[38] Barmenkov YO, Zalvidea D, Torres-Peiró S, Cruz JL, Andrés MV. Effective length of short Fabry-Perot cavity formed by uniform fiber Bragg gratings. Opt Express 2006;14(14):6394–9. https://doi.org/10.1364/OE.14.006394.

[39] Barmenkov YO, Cruz JL, Díez A, Andrés MV. Electrically tunable photonic true-time-delay line. Opt Express 2010;18(17):17859–64. https://doi.org/10.1364/OE.18.017859.

[40] Ferreira MFS, Paul MC, eds. Optical Fiber Technology and Applications. Chapter 3. IOP publishing 2021. ISBN: 978-0-7503-3241-5. https://doi.org/10.1088/978-0-7503-3243-9ch3.

[41] Miao Y, Zhang H, Xiao H, Zhou P, Liu Z. 1150-nm Yb-doped fiber laser pumped directly by laser-diode with an output power of 52 W. IEEE Phot Technol Lett 2014; 26(23):2327–3239. https://doi.org/10.1109/LPT.2014.2355222.